Supporting Information

Sulfide-oxidation-assisted electrochemical water splitting for H_2 production on a bifunctional Cu_2S/nickel foam catalyst

Yuhou Pei,[a] Jiong Cheng,[a] Heng Zhong,*[a,b,c] Zhenfeng Pi,[a] Yu Zhao[d] and Fangming Jin[a,b,c]

[a] School of Environmental Science and Engineering, State Key Lab of Metal Matrix Composites, Shanghai Jiao Tong University, Shanghai 200240, P.R. China

[b] Center of Hydrogen Science, Shanghai Jiao Tong University, Shanghai, 200240, P.R. China

[c] Shanghai Institute of Pollution Control and Ecological Security, Shanghai 200092, P.R. China

[d] School of Electronic Information and Electrical Engineering, Shanghai Jiao Tong University, Shanghai 200240, P.R. China

*Corresponding: zhong.h@sjtu.edu.cn

Experimental Section

Chemicals.

Metal nitrates ($Cu(NO_3)_2 \cdot 3H_2O$ (99.0%), $Ni(NO_3)_2 \cdot 6H_2O$ (98.0%), $Co(NO_3)_2 \cdot 6H_2O$ (98.5%), and $Fe(NO_3)_3 \cdot 9H_2O$ (98.5%)), urea (99.0%), and NaOH (96.0%) were purchased from Sinopharm Chemical Reagent Co,. Ltd. $Na_2S \cdot 9H_2O$ (98.0%) was purchased from Shanghai Lingfeng Chemical Reagent Co. Ltd. The Pt/C (20 wt%) was purchased from Innochem Chemical Reagent Co. Ltd. All chemicals employed in this work were used directly without any further purification.

Material characterization.

Morphology and elemental dispersion of the electrode materials were observed by a field-emission scanning electronic microscopy (SEM, Zeiss, Sigma 500, 10 kV) with an energy dispersion X-ray spectroscopy (EDX) and a transmission electronic microscopy (TEM, JEOL, JEM 2100F, 200 kV). Crystal phases of electrode materials were measured by a Bruker D8 advance X-ray diffraction (XRD) instrument (Cu Kα radiation, λ = 1.5406 Å) with a scanning rate of 2^o min^{-1} from 10^o to 80^o (2θ). X-ray photoelectron spectroscopy (XPS) was conducted on a ThermoFisher 250Xi XPS analyzer (Al Kα, 1486.6 eV). The binding energies of XPS results were calibrated by C1s peak at 284.6 eV. UV-visible (MAPADA UV-3100PC) spectrum was employed to test the anodic products of polysulfides. Inductively Coupled Plasma-Atomic Emission Spectrometry (ICP-AES, Thermo Scientific, iCAP7600) was used for element analysis.

Hydrogen production analysis.

Hydrogen production was analyzed by a gas chromatography equipped with a thermal conductivity detector (GC-TCD, Agilent, 7890A). Ar gas was continuously purged into cathodic electrolyte (1 mol L^{-1} NaOH) at a rate of 5 sccm, and the gas products were collected by a water-gas replacing method. The Faradaic efficiency of H_2 production was calculated based on the following equation (1):

$$FE(\%) = \frac{2Fn}{It} \times 100\%, \quad (1)$$

where F is Faradaic constant (96485 C mol^{-1}), n is the amount of produced hydrogen gas (mol), I is the current (A), and t is the time (s) of electrolysis.

Recovery of elementary S by acidification.

Anodic electrolyte after the SOR reaction was placed into an ice bath and was added with concentrated sulfuric acid dropwise until the *p*H changed to 1.0 to form yellow precipitates. The solid yellow products were then collected by filtration, washed by DI water, and dried at 50 ^{o}C in the oven for further analysis.

Calculation details

The theoretical calculations were performed using Vienna Ab-initio Simulation Package (VASP).[S1-3] The projector-augmented-wave (PAW) method was adopted for the pseudopotentials,[S4] and cut-off energy was set to 400 eV. The Perdew-Burke-Ernzerhof (PBE) exchange-correlation functional within the generalized gradient approximation (GGA) was used to describe the exchange-correlation energy.[S5] The convergence force and energy were set as 0.05 eV/Å and 0.001 eV, respectively. The spin-polarization was considered during the calculations. The monoclinic Cu_2S slabs were established as the calculation models.[S6-8] The free energies of SOR steps were calculated by the equation: $\Delta G = \Delta E_{DFT} + \Delta E_{ZPE} - T\Delta S$, where ΔE_{DFT} is the DFT energy difference, the ΔE_{ZPE} and ΔS are obtained by the zero-point energy correction and analysis of the variation of entropy, respectively.

Table S1 Redox potentials of related substances in this work.[S9]1

Redox couple	Potential (V vs. SHE)
$Cu(OH)_2/Cu_2O$	-0.08
Ni^{2+}/Ni	-0.26
$Fe(OH)_3/Fe(OH)_2$	-0.56
$Co(OH)_2/Co$	-0.73

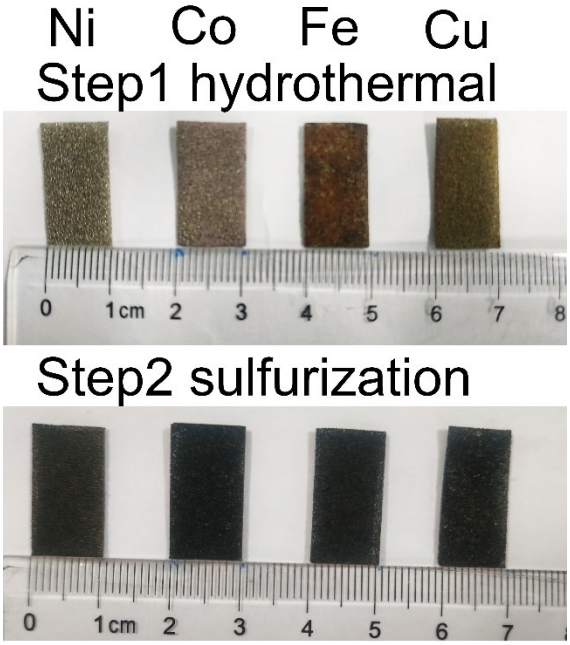

Figure S1 Photograph of metal (hydr-)oxides before (upper row) and after sulfurization (lower row) (the electrodes were fabricated via a hydrothermal step followed by a sulfurization step at room temperature).

Table S2 K_{sp} values of metal (hydr-)oxides and corresponding sulfides. [S9-S13]1-5

(Hydr-)oxides	K_{sp}	Sulfides	K_{sp}
Cu_2O	2.0×10^{-15}	Cu_2S	2.5×10^{-48}
$Ni(OH)_2$	5.9×10^{-16}	NiS	1.0×10^{-24}
$Co(OH)_2$	5.9×10^{-15}	CoS	2.0×10^{-25}
$Fe(OH)_3$	2.8×10^{-39}	Fe_2S_3	1.0×10^{-88}

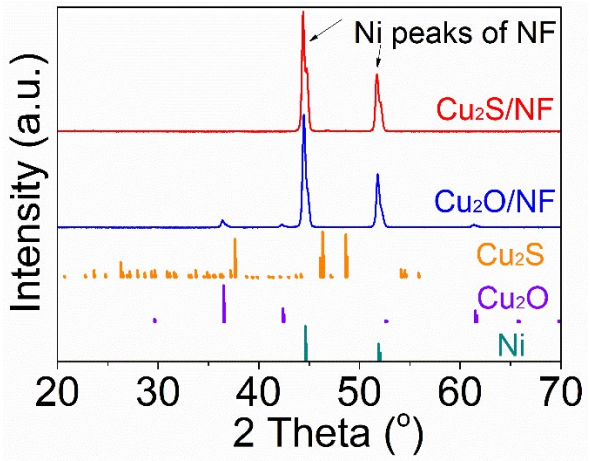

Figure S2 XRD patterns of the Cu_2O/NF and Cu_2S/NF electrodes at the full scale of intensity (partial magnified image can be found in Fig. 1b of the main text).

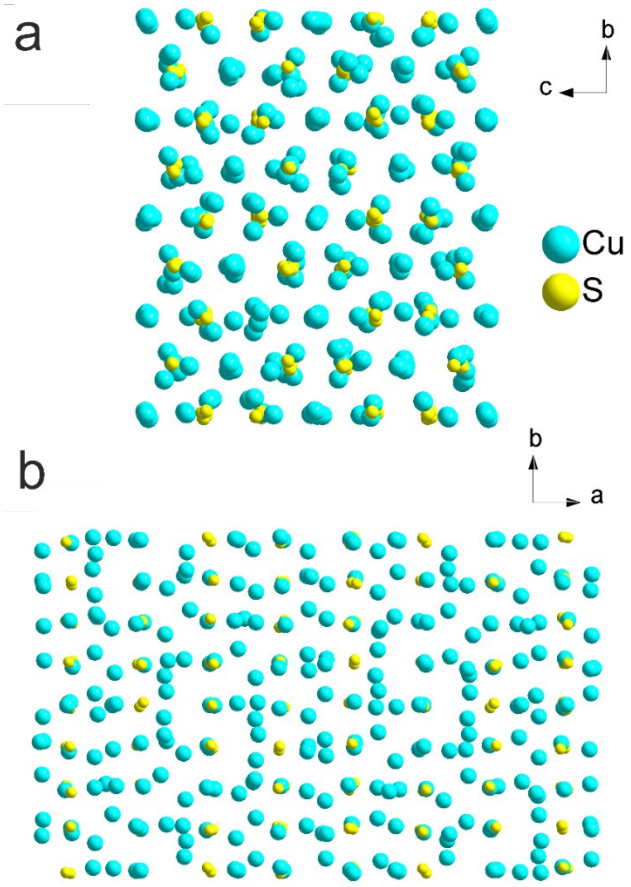

Figure S3 Crystal structure of monoclinic $Cu_{31}S_{16}$ from the view along **a** and **c**-axis. Space group P21/n, a=26.897 Å, b=15.745 Å, c=13.465 Å.

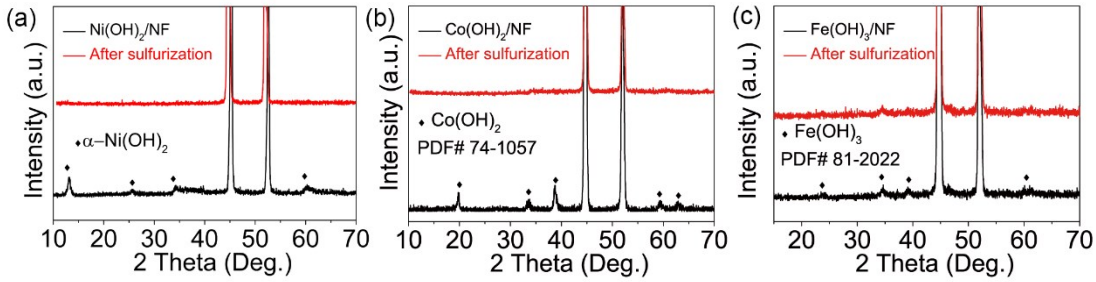

Figure S4 XRD patterns of $Ni(OH)_2$/NF, $Co(OH)_2$/NF, $Fe(OH)_3$/NF, and corresponding Ni-S/NF, Co-S/NF, and Fe-S/NF electrodes after sulfurization.

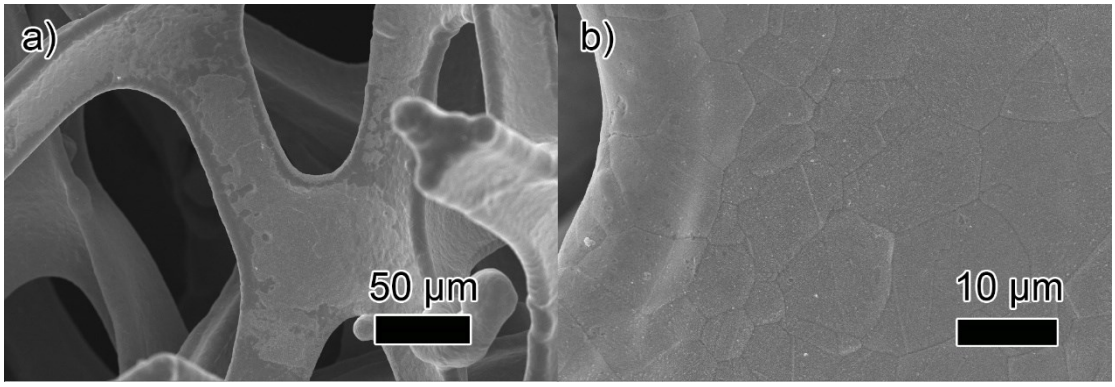

Figure S5 SEM images of nickel foam.

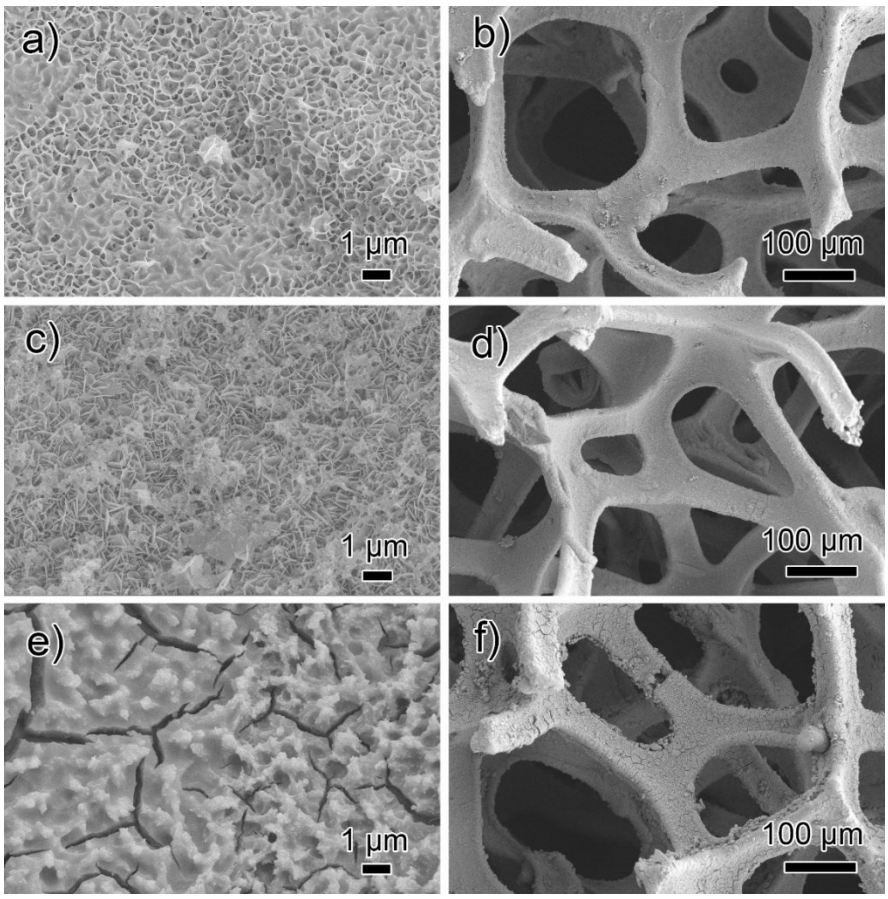

Figure S6 SEM images of sulfurized Ni-S/NF (a, b), Co-S/NF (c, d), and Fe-S/NF (e, f) catalysts.

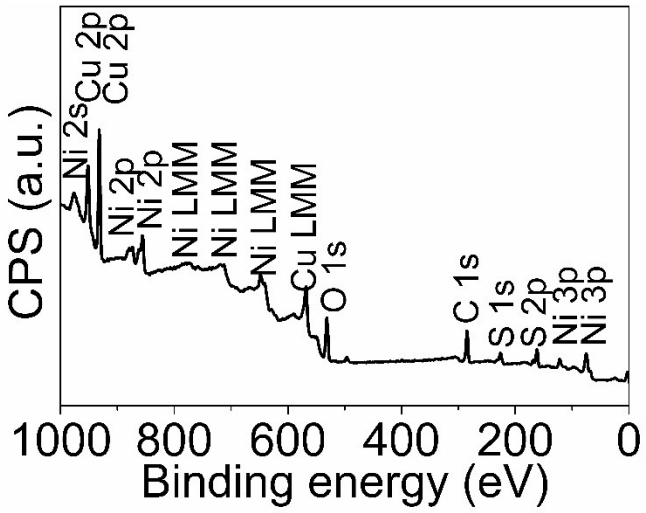

Figure S7 Wide scan XPS spectra of the Cu_2S/NF electrode.

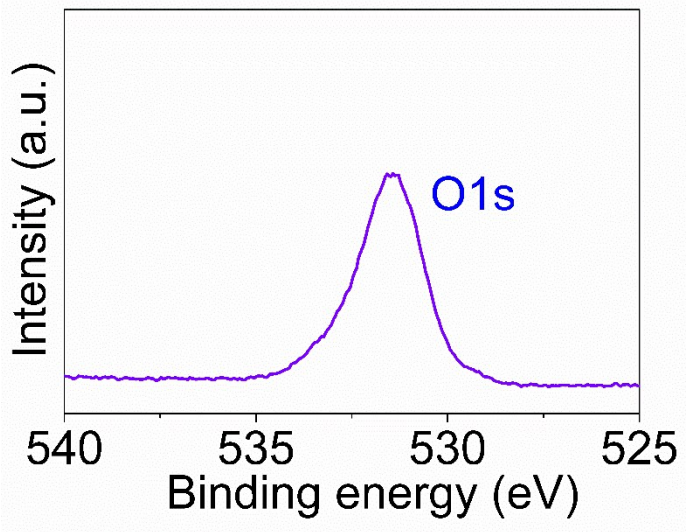

Figure S8 XPS spectrum of O1s for the Cu_2S/NF electrode.

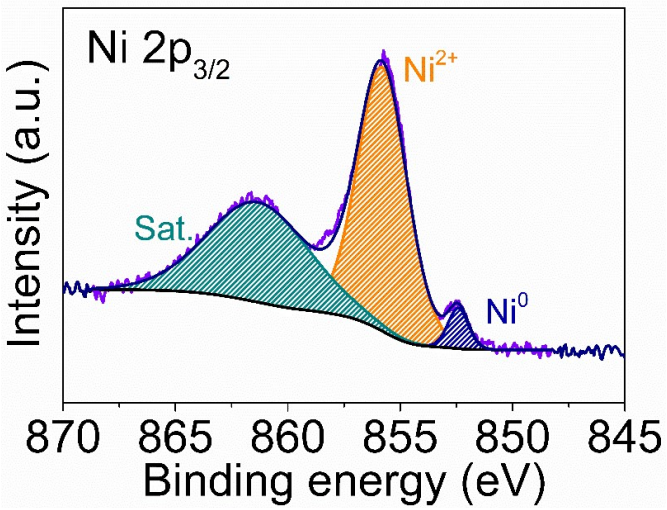

Figure S9 XPS spectrum of Ni $2p_{3/2}$ for the Cu_2S/NF electrode.

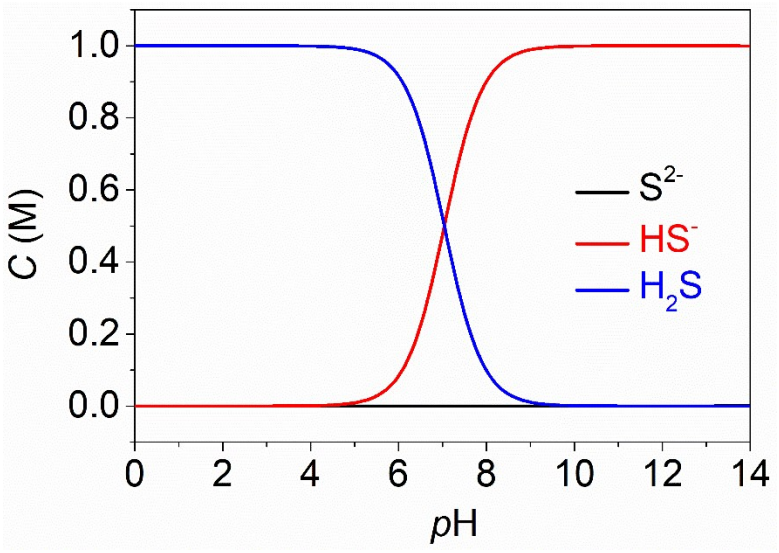

Figure S10 Relationship between *p*H value (0-14) and concentrations of H_2S and HS^- at a concentration of 1 mol L^{-1} total S species based on pKa_1 = 7.04 and pKa_2 = 17.10.[S14,S15]

Table S3 ICP analysis of NaOH and Na_2S used in electrolyte.

	NaOH (wt%)	Na_2S (wt%)		NaOH (wt%)	Na_2S (wt%)
Al	0.000	0.001	Mn	0.000	0.000
As	0.000	0.000	Na	48.841	18.549
B	0.000	0.000	Ni	0.000	0.000
Be	0.000	0.000	P	0.000	0.000
Ba	0.000	0.000	Pb	0.000	0.000
Bi	0.001	0.002	Se	0.001	0.001
Ca	0.000	0.004	Sr	0.000	0.000
Cd	0.000	0.000	V	0.000	0.000
Co	0.000	0.000	Zn	0.000	0.000
Cr	0.000	0.000	Mo	0.000	0.000
Cu	0.000	0.000	Pd	0.000	0.000
Fe	0.000	0.000	Re	0.000	0.000
K	0.023	0.004	S	0.000	9.226
Li	0.000	0.000	Sb	0.000	0.000
Mg	0.000	0.000	Si	0.000	0.000
Ti	0.000	0.000	W	0.000	0.000

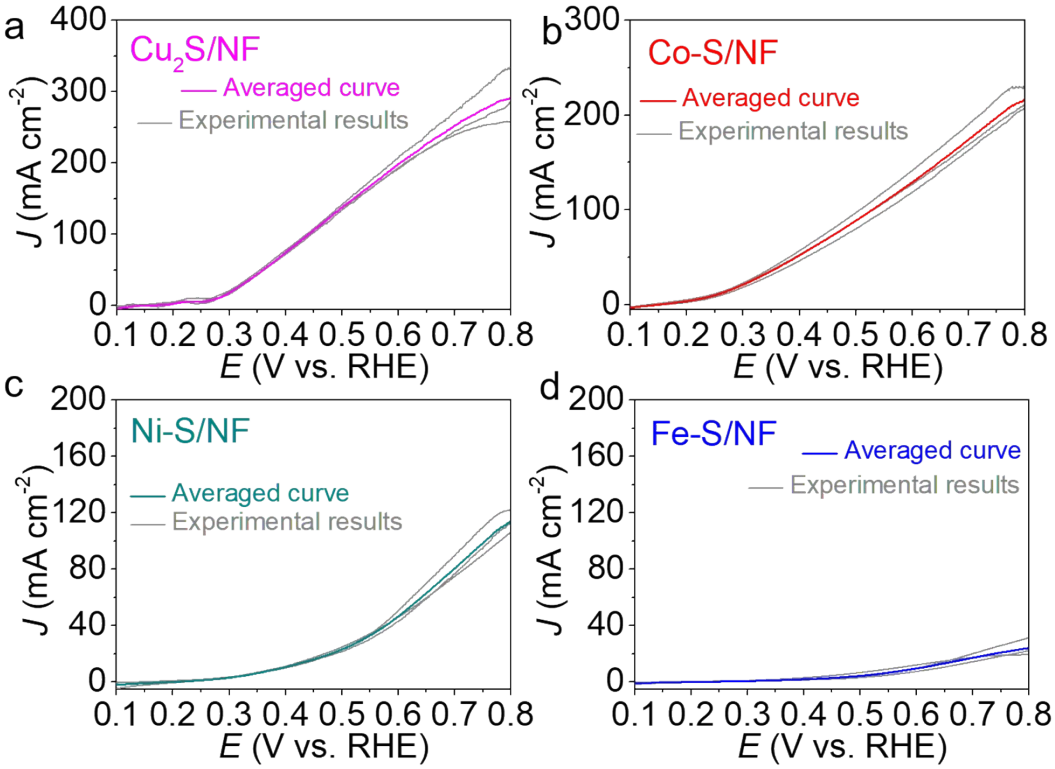

Figure S11 LSV reproducibility test of the fabricated **a** Cu_2S/NF, **b** Co-S/NF, **c** Ni-S/NF, and **d** Fe-S/NF electrodes for the SOR (each experiment was repeated three independent times, including electrode fabrication and electrochemical test).

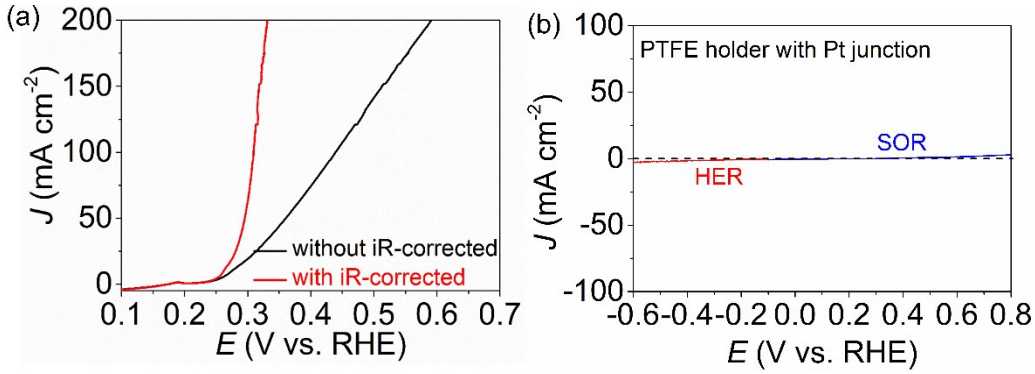

Figure S12 (a) LSV curves of Cu_2S/NF electrode in 1 mol L^{-1} NaOH + 1 mol L^{-1} Na_2S electrolyte at a scan rate of 5 mV s^{-1} (R_s (resistance of the solution) in this system was tested to be 1.3 Ω). (b) Electrochemical effect of the PTFE holder with a Pt plate toward HER and SOR without electrodes.[S16]

Table S4 Comparison of the current densities obtained at different potentials on various electrodes for SOR reactions[a]

Catalysts	Reaction conditions	Current density ($mA\ cm^{-2}$)	E (V) vs. RHE	Ref.
Cu_2S/NF	1 M NaOH +1M Na_2S	10 100	0.26 0.44	**This work**
CoNi@NGs	1 M NaOH +1M Na_2S	10 100	0.34 0.52	[S17]
$NiCoO_x$-CNTs	1 M NaOH +1M Na_2S	10 50	0.37 0.50	[S17]
IrO_2	1 M NaOH +1M Na_2S	10	0.43	[S17]
Graphite electrode	1 M NaOH+ 1M NaHS+2 M NaCl[b]	10 100	0.34 0.51	[S18]
Pt electrode	0.1 M Na_2S + 1 M NaOH	0.1	1.8	[S19]
CoP nanoarray	1 M NaOH +50 mM Na_2S	10 20	1.27 1.31	[S20]
Ir mixed-metal oxide (Ir-MMO)	1 M NaOH +1M Na_2S	30	0.91	[S21]
Ru MMO	50 mM NaOH +50 mM Na_2S	5	1.62	[S22]
TaO_2/IrO_2	1.6 M NaOH +130 mM Na_2S	10	2.74 (cell)	[S23]
Pt disk	1M Na_2S	100	1.0 (vs SCE)	[S24]
Carbon cloth	5 mM Na_2S + 100 mM PBS	0.43	1.0	[S25]

[a] The reactions were performed at room temperature without specific instruments.
[b] reaction occurred at 80 ^oC.

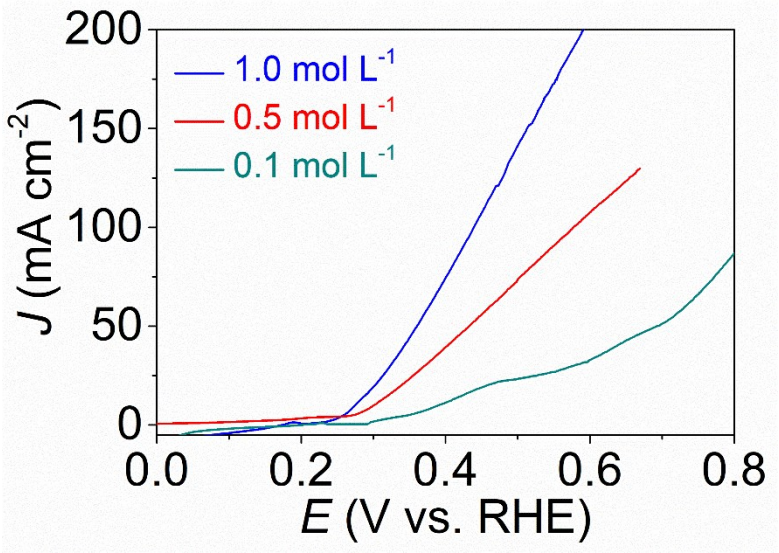

Figure S13 LSV curves obtained on Cu_2S/NF in the electrolyte containing 1 mol L^{-1} NaOH with 0.1, 0.5, and 1.0 mol L^{-1} Na_2S.

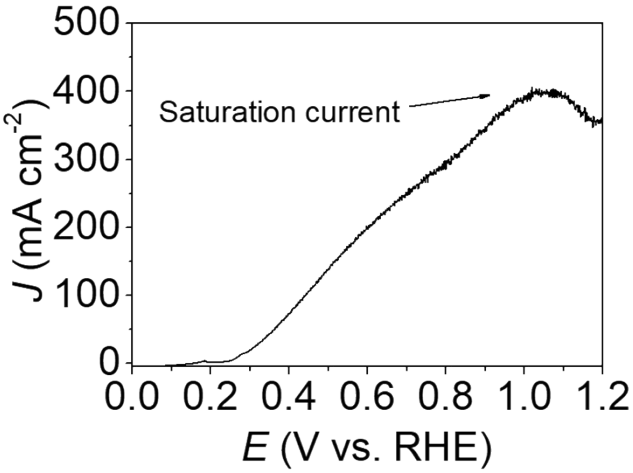

Figure S14 LSV curve of the Cu_2S/NF electrode with a wide potential window from 0 to 1.2 V vs. RHE. Electrolyte: 1 mol L^{-1} NaOH + 1 mol L^{-1} Na_2S in water solution; scan rate: 5 mV s^{-1}.

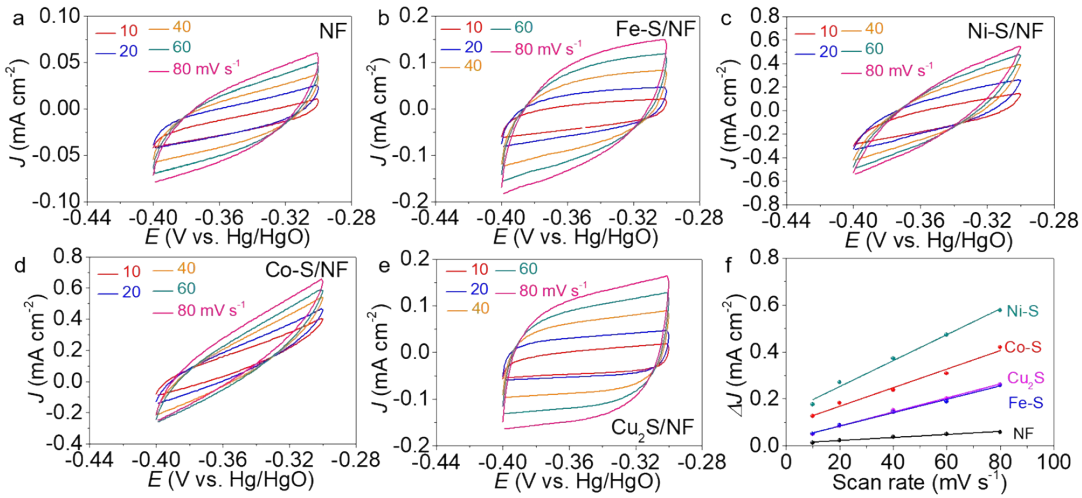

Figure S15 (a-e) ECSA measurements of electrodes at different scan rate from 10 to 80 mV s^{-1}, and (f) corresponding linear fitting of the relationship between scan rates and current densities.

Table S5 ECSA results of electrodes based on Figure S15.

Electrode	C (mF cm^{-2})
Ni-S/NF	5.42
Co-S/NF	3.91
Cu_2S/NF	2.87
Fe-S/NF	2.74
NF	0.68

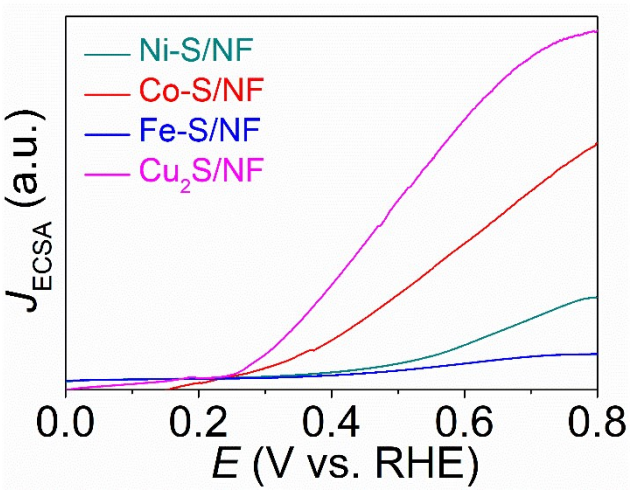

Figure S16 LSV curves based on ECSA results.

Table S6 Parameters of ionization potential (***I***), electron affinity (***A***), and absolute hardness (η) of selected cations[a]

Cations	***I*** **(eV)**	***A*** **(eV)**	$\eta=(I-A)/2$ **(eV)**	**Soft or hard**
Cu^{+}	20.29	7.73	6.28	Soft
Co^{2+}	33.50	17.06	8.22	Borderline
Ni^{2+}	35.71	18.17	8.50	
Fe^{3+}	54.80	30.65	12.08	Hard

[a] Data obtained from Ref. [S26]

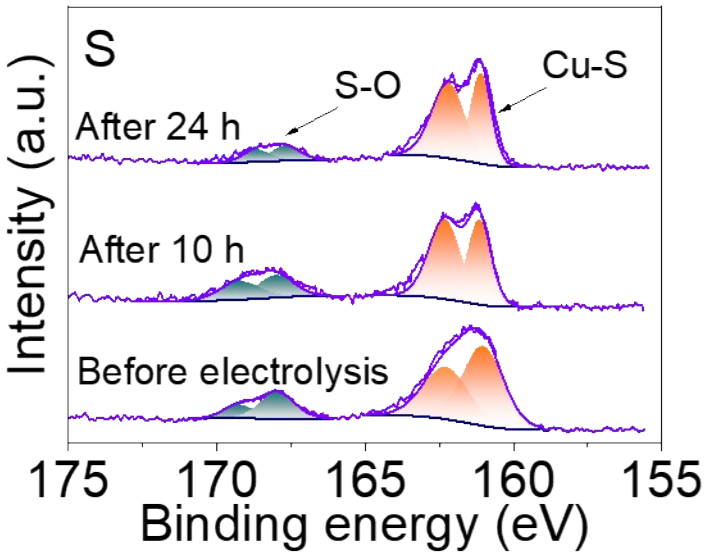

Figure S17 XPS spectra of S of the Cu_2S/NF electrodes before and after electrolysis at 100 mA cm^{-2} for 10 and 24 h.

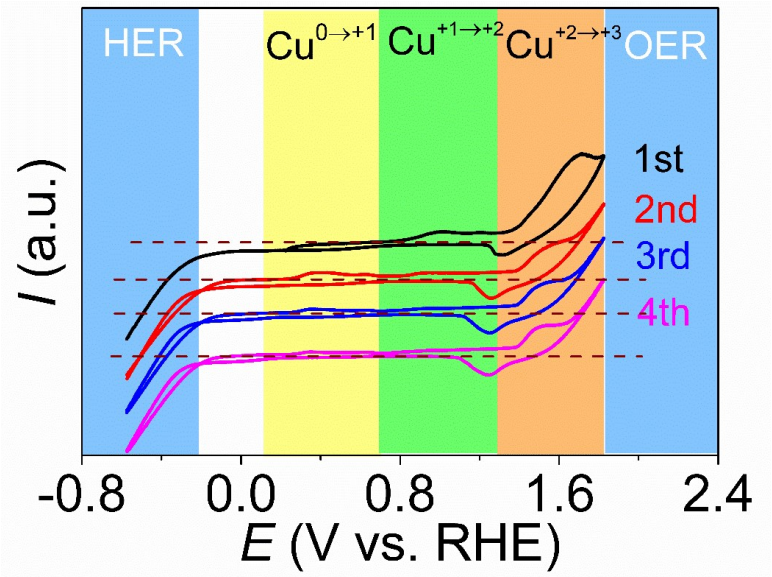

Figure S18 CV curves of Cu_2S/NF electrode in 1 mol L^{-1} NaOH electrolyte from -0.6 to 1.8 V at a scan rate of 5 mV s^{-1}.

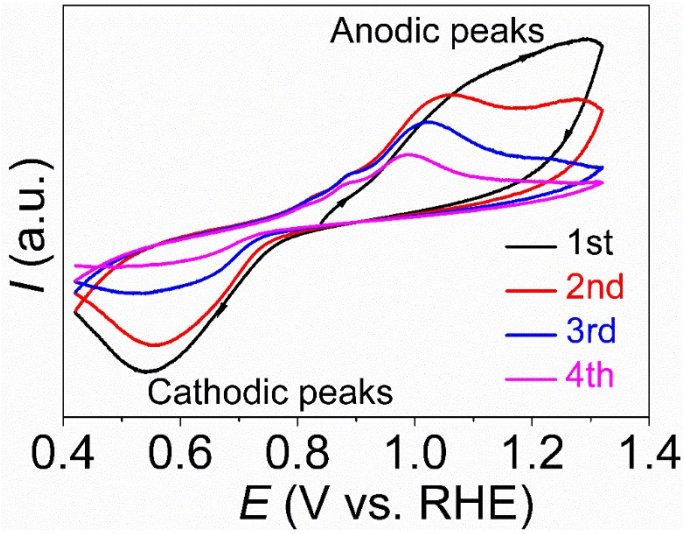

Figure S19 CV curves of Cu_2S/NF electrode in 1 mol L^{-1} NaOH electrolyte from 0.4 to 1.3 V at a scan rate of 10 mV s^{-1}.

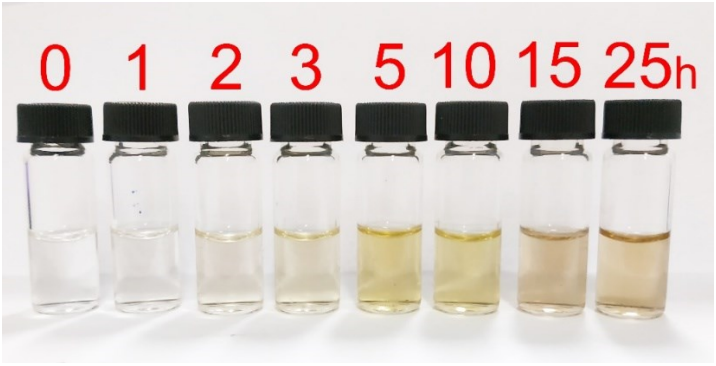

Figure S20 Photographs of anodic electrolytes (diluted for 40 times) after SOR for 0 to 25 h on Cu_2S/NF at a constant current density of 100 mA cm^{-2}.

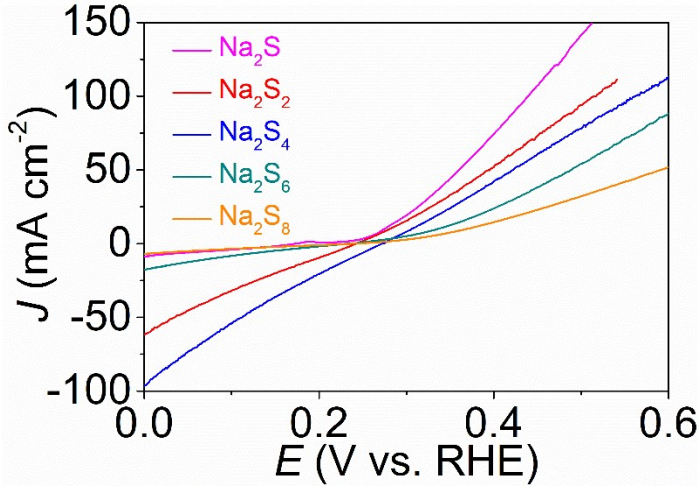

Figure S21 LSV curves of the polysulfide electrooxidation reactions on the Cu_2S/NF electrode. Electrolytes: 1 mol L^{-1} NaOH + 1 mol L^{-1} polysulfide (Na_2S_x, synthesized by stoichiometrically blending elemental sulfur and Na_2S in alkaline medium to form clear solution, $HS^- + (n-1)/8S_8 + OH^- = S_n^{2-} + H_2O$).

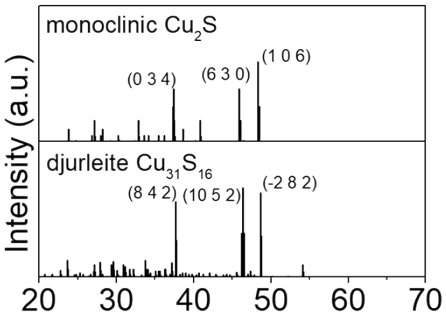

Figure S22 Standard XRD patterns of the monoclinic Cu_2S (PDF#33-490) and djurleite $Cu_{31}S_{16}$ (PDF#34-660).

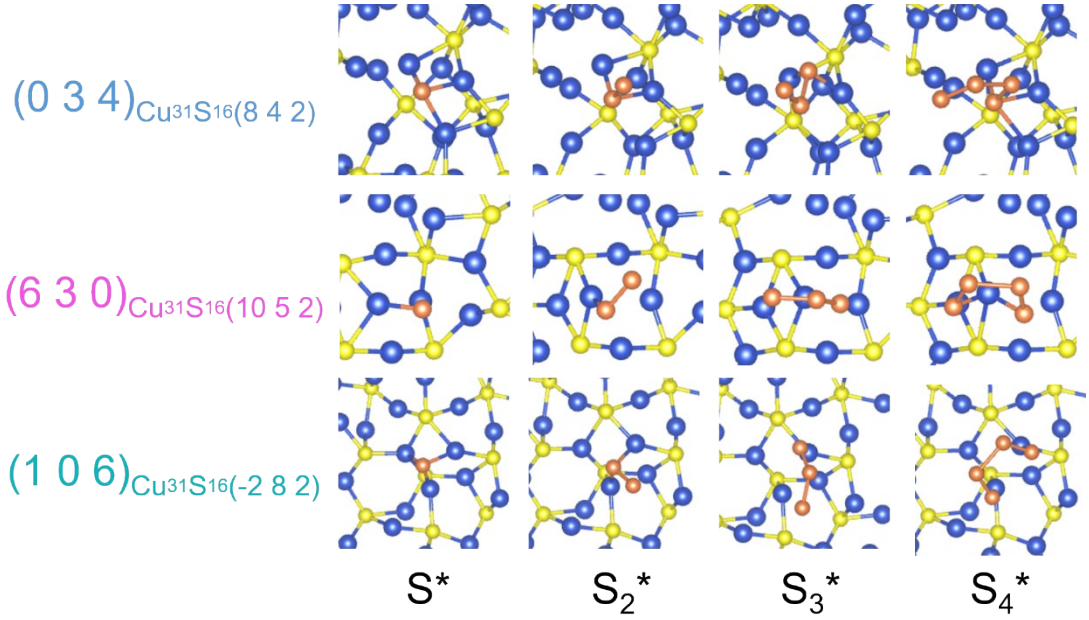

Figure S23. Schematic diagram of the adsorption states of S_x^* (x = 1, 2, 3, 4) on the (0 3 4)$_{Cu31S16(8\ 4\ 2)}$, (6 3 0)$_{Cu31S16(10\ 5\ 2)}$, and (1 0 6)$_{Cu31S16(-2\ 8\ 2)}$ facets.

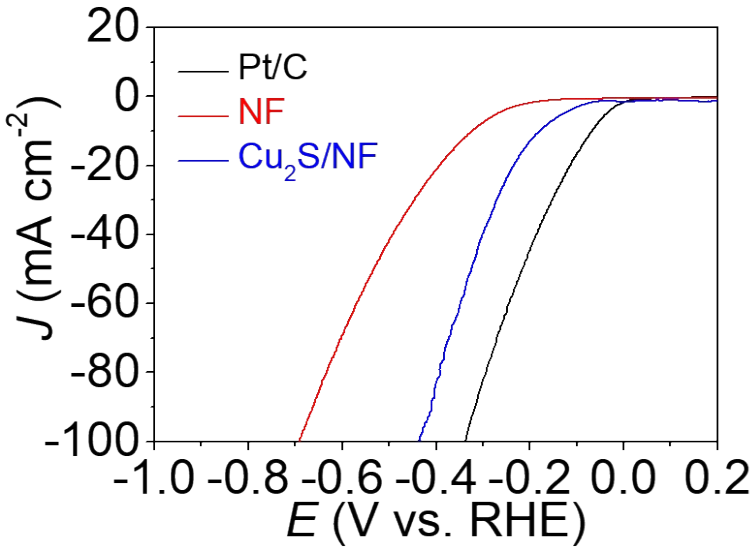

Figure S24 LSV curves (without *iR*-corrected) obtained in 1 mol L^{-1} NaOH on Cu_2S/NF, NF, and Pt/C for HER at a scan rate of 5 mV s^{-1}.

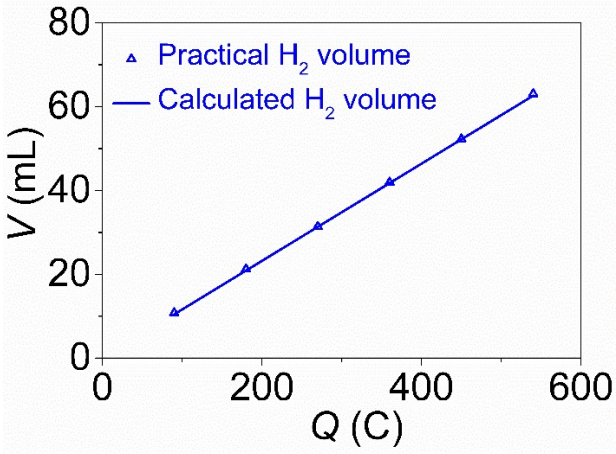

Figure S25 Comparison between the theoretical and practical H_2 evolution.

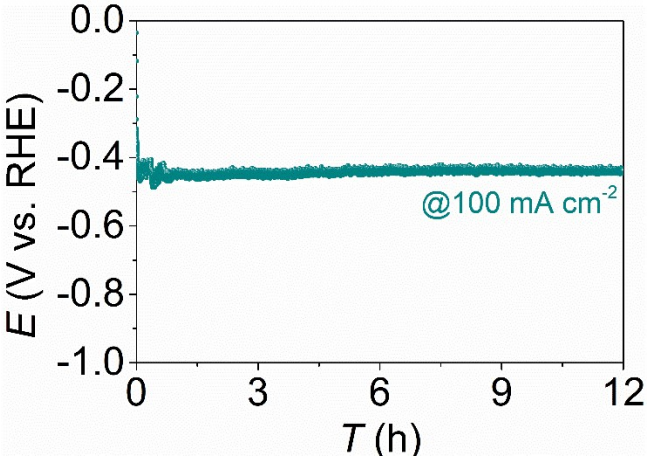

Figure S26 Potential-time test of HER at the current density of 100 mA cm^{-2} catalyzed by the Cu_2S/NF electrode in 1 mol L^{-1} NaOH for 12 h.

Table S7 Comparison of several room-temperature electrolytic hydrogen production systems in alkaline medium.

No.	Catalyst system	Anodic electrolyte	Anodic Product	E_{COR} (V) [a]	E_C (V) [b]	Current density [c] (mA cm^{-2})	Ref.
1	CoS_2/MoS_2|| CoS_2/MoS_2	1 M KOH + 0.5 M urea	N_2	1.29	1.29	10	[S27]
2	$NiTe_2/Ni(OH)_2$	1 M KOH +0.33 M urea	N_2	1.35	NG [d]	10	[S28]
3	Ni_2P/NF||Ni_2P/NF	1.0 M KOH + 10 mM HMF	FDCA	~1.35	1.44	10	[S29] 15
4	MoO_2-FeP@C|| MoO_2-FeP@C	1.0 M KOH + 10 mM HMF	FDCA	1.35	1.48	10	[S31] 16
5	$Co(OH)_2$@HOS/CP|| $Co(OH)_2$@HOS/CP	1.0 M KOH + 3 M methanol	Formate	1.38	1.49	10	[S13] 6
6	$Ni_{0.33}Co_{0.67}(OH)_2$/NF|| $Ni_{0.33}Co_{0.67}(OH)_2$/NF nanoneedle	1.0 M KOH + 0.5 M methanol	Formate	~1.35	1.50	10	[S33]
7	Ni-Mo-N/CFC||Ni-Mo-N/CFC	1.0 M KOH + 0.1 M glycerol	Formate	1.30	1.36	10	[S32]
8	PtCu||PtCu catalyst	1.0 M KOH + CO	CO_2	~0.5	NG [d]	50	[S34]
9	Ni_2P||Ni_2P	1 M KOH+ 0.5 mM THIQs	DHIQs	~1.3	~1.4	10	[S36]
10	Ni_2P ||Ni_2P	1.0 M KOH + 0.125 M Benzylamine	Benzonit-rile	1.34	1.41	10	[S37]
11	Graphite||CoNi@NGs	1.0 M NaOH+ 1.0 M Na_2S	Sulfur	~0.35	NG [d]	10	[S17]
12	**Cu_2S/NF||Cu_2S/NF**	**1.0 M NaOH+1.0 M Na_2S**	**Sulfur**	**0.26**	**0.43**	**10**	**This work**
13	**Cu_2S/NF||Cu_2S/NF**	**1.0 M NaOH+ 1.0 M Na_2S**	**Sulfur**	**0.29**	**0.53**	**30**	**This work**
14	**Cu_2S/NF||Cu_2S/NF**	**1.0 M NaOH+ 1.0 M Na_2S**	**Sulfur**	**0.32**	**0.64**	**100**	**This work**

[a] E_{COR}: anodic potential of chemical oxidation reaction, vs RHE.

[b] E_C: cell voltage.

[c] Current density: current density for E_{COR} and E_C.

[d] NG: not given.

References

S1. Kresse, G.; Furthmüller, J., Efficiency of ab-initio total energy calculations for metals and semiconductors using a plane-wave basis set. *Computational Materials Science* **1996**, *6*(1), 15-50.

S2. Blöchl, P. E., Projector augmented-wave method. *Physical review B* **1994**, 50(24), 17953.

S3. Kresse, G.; Furthmüller, J., Efficient iterative schemes for ab initio total-energy calculations using a plane-wave basis set. *Physical review B* **1996**, *54*(16), 11169.

S4. Kresse, G.; Hafner, J., Ab initio molecular-dynamics simulation of the liquid-metal–amorphous-semiconductor transition in germanium. *Physical Review B* **1994**, *49*(20), 14251.

S5. Perdew, J. P.; Chevary, J. A.; Vosko, S. H.; Jackson, K. A.; Pederson, M. R.; Singh, D. J.; Fiolhais, C., Atoms, molecules, solids, and surfaces: Applications of the generalized gradient approximation for exchange and correlation. *Physical review B* **1992**, 46 (11), 6671.

S6. Kim, M.-C.; Nam, H.; Choi, J.; Kim, H. S.; Lee, H. W.; Kim, D.; Kong, J.; Han, S. S.; Lee, S. Y.; Park, H. S., Hydrogen bonding-mediated enhancement of bioinspired electrochemical nitrogen reduction on $Cu_{2-x}S$ catalysts. *ACS Catal.* **2020**, *10*(18), 10577-10584.

S7. Evans, H. T., Crystal structure of low chalcocite. *Nature Physical Science* **1971**, *232*(29), 69-70.

S8. Chen, L.; Hu, H.; Chen, Y.; Gao, J.; Li, G., Plasmonic $Cu_{2-x}S$ nanoparticles: a brief introduction of optical properties and applications. *Materials Advances* **2021**.

S9. Lide, D. R., *CRC Handbook of Chemistry and Physics*. CRC press: **2004**; Vol. 85.

S10. He, H. Y.; Fei, J.; Lu, J., Chemical Bath Deposition and Optical and Electrical Properties of Pure and Doped Fe_2S_3 Films. *Micro and Nanosystems* **2014,** *6*(2), 126-132.

S11. Ye, L.; Wen, Z.; Li, Z.; Huang, H., Hierarchical Architectured Ternary

Nanostructures Photocatalysts with $In(OH)_3$ Nanocube on $ZnIn_2S_4$/NiS Nanosheets for Photocatalytic Hydrogen Evolution. *Solar RRL* **2020**, *4*, 2000027.

S12. Zuo, Y.; Liu, Y.; Li, J.; Du, R.; Han, X.; Zhang, T.; Arbiol, J.; Divins, N. J.; Llorca, J.; Guijarro, N.; Sivula, K.; Cabot, A., In Situ Electrochemical Oxidation of Cu_2S into CuO Nanowires as a Durable and Efficient Electrocatalyst for Oxygen Evolution Reaction. *Chemistry of Materials* **2019,** *31*(18), 7732-7743.

S13. Xiang, K.; Wu, D.; Deng, X.; Li, M.; Chen, S.; Hao, P.; Guo, X.; Luo, J. L.; Fu, X. Z., Boosting H_2 Generation Coupled with Selective Oxidation of Methanol into Value-Added Chemical over Cobalt Hydroxide@Hydroxysulfide Nanosheets Electrocatalysts. *Advanced Functional Materials* **2020**, *30*, 1909610.

S14 May, P. M., Batka, D., Hefter, G., Konigsberger, E., Rowland, D., *Chemical Communications* **2018**, *54*, 1980-1983.

S15 Grethlein, A., Soni, B., Worden, R., Jain, M., *Applied Biochemistry and Biotechnology* **1992**, *34*, 233.

S16 Zheng, W.; Liu, M.; Lee, L. Y. S., Best Practices in Using Foam-Type Electrodes for Electrocatalytic Performance Benchmark. *ACS Energy Letters* **2020**, *5* (10), 3260-3264.

S17 Zhang, M.; Guan, J.; Tu, Y.; Chen, S.; Wang, Y.; Wang, S.; Yu, L.; Ma, C.; Deng, D.; Bao, X., Highly Efficient H_2 Production from H_2S via a Robust Graphene-Encapsulated Metal Catalyst. *Energy & Environmental Science* **2020**, *13*(1), 119-126.

S18 Petrov K., Srinivasan S., Low temperature removal of hydrogen sulfide from sour gas and its utilization for hydrogen and sulfur production. *International Journal of Hydrogen Energy* **1996**, *21*, 163-169.

S19 Sanli A E, Yılmaz O, Aytaç A, A novel H_2S/H_2O_2 fuel cell operating at the temperature of 298 K. *International Journal of Energy Research* **2013**, *37*, 1205-1212.

S20 Hao S, Yang L, Liu D, et al., Replacing oxygen evolution with sodium sulfide electro-oxidation toward energy-efficient electrochemical hydrogen production: Using cobalt phosphide nanoarray as a bifunctional catalyst. *International Journal of Hydrogen Energy* **2017**, *42*, 26289-26295.

S21 Ntagia E, Fiset E, Truong Cong Hong L, Vaiopoulou E, Rabaey K,

Electrochemical treatment of industrial sulfidic spent caustic streams for sulfide removal and caustic recovery. *Journal of Hazardous Material* **2020**, *388*, 121770.

S22 Ntagia E, Fiset E, da Silva Lima L, et al., Anode materials for sulfide oxidation in alkaline wastewater: An activity and stability performance comparison. *Water Research* **2019**, *149*, 111-119.

S23 Vaiopoulou E, Provijn T, Prevoteau A, Pikaar I, Rabaey K, Electrochemical sulfide removal and caustic recovery from spent caustic streams. Water Research **2016**, *92*, 38-43.

S24 Zhao Y, Wang S, Varela H, et al., Spatiotemporal Pattern Formation in the Oscillatory Electro-Oxidation of Sulfide on a Platinum Disk. *The Journal of Physical Chemistry C* **2011**, *115*, 12965-12971.

S25 Lin H, Williams N, King A, Hu B, Electrochemical sulfide removal by low-cost electrode materials in anaerobic digestion. *Chemical Engineering Journal* **2016**, *297*, 180-192.

S26 Pearson, R. G., Absolute Electronegativity and Hardness: Application to Inorganic Chemistry. *Inorganic Chemistry* **1988,** *27*(4), 734-740.

S27 Li, C.; Liu, Y.; Zhuo, Z.; Ju, H.; Li, D.; Guo, Y.; Wu, X.; Li, H.; Zhai, T., Local Charge Distribution Engineered by Schottky Heterojunctions toward Urea Electrolysis. *Advanced Energy Materials* **2018**, *8*(27), 1801775.

S28 Xu, B.; Yang, X.; Liu, X.; Song, W.; Sun, Y.; Liu, Q.; Yang, H.; Li, C., Lattice Distortion in Hybrid $NiTe_2/Ni(OH)_2$ Nanosheets as Efficient Synergistic Electrocatalyst for Water and Urea Oxidation. *Journal of Power Sources* **2020**, *449*, 227585.

S29 You, B.; Jiang, N.; Liu, X.; Sun, Y., Simultaneous H_2 Generation and Biomass Upgrading in Water by an Efficient Noble-Metal-Free Bifunctional Electrocatalyst. *Angewandte Chemie International Edition* **2016,** *128*, 10067-10071.

S30 Zhao, Y.; Jia, N.; Wu, X.-R. Li, F.-M.; Chen, P.; Jin, P.-J.; Yin, S.; Chen, Y., Rhodium Phosphide Ultrathin Nanosheets for Hydrazine Oxidation Boosted Electrochemical Water Splitting. *Applied Catalysis B: Environmental* **2020**, *270*, 118880.

S31 Yang, G.; Jiao, Y.; Yan, H.; Xie, Y.; Wu, A.; Dong, X.; Guo, D.; Tian, C.; Fu, H., Interfacial Engineering of MoO_2-FeP Heterojunction for Highly Efficient Hydrogen Evolution Coupled with Biomass Electrooxidation. *Advanced Materials* **2020**, *32*, 2000455.

S32 Li, Y.; Wei, X.; Chen, L.; Shi, J.; He, M., Nickel-molybdenum Nitride Nanoplate Electrocatalysts for Concurrent Electrolytic Hydrogen and Formate Productions. *Nature Communications* **2019,** *10*, 5335.

S33 Li, M.; Deng, X.; Xiang, K.; Liang, Y.; Zhao, B.; Hao, J.; Luo, J. L.; Fu, X. Z., Value-added Formate Production from Selective Methanol Oxidation as A Novel Anodic Reaction to Enhance Electrochemical Hydrogen Co-generation. *ChemSusChem* **2019**, *13*(5), 914-921..

S34 Cui, X.; Su, H. Y.; Chen, R.; Yu, L.; Dong, J.; Ma, C.; Wang, S.; Li, J.; Yang, F.; Xiao, J.; Zhang, M.; Ma, D.; Deng, D.; Zhang, D. H.; Tian, Z.; Bao, X., Room-temperature Electrochemical Water-gas Shift Reaction for High Purity Hydrogen Production. *Nature Communications* **2019,** *10*, 86.

S35 Hao, S.; Yang, L.; Liu, D.; Kong, R.; Du, G.; Asiri, A. M.; Yang, Y.; Sun, X., Integrating Natural Biomass Electro-oxidation and Hydrogen Evolution: Using a Porous Fe-doped CoP Nanosheet Array as a Bifunctional Catalyst. *Chemical Communications* **2017,** *53*(42), 5710-5713.

S36 Huang, C.; Huang, Y.; Liu, C.; Yu, Y.; Zhang, B., Integrating Hydrogen Production with Aqueous Selective Semi-Dehydrogenation of Tetrahydroisoquinolines over a Ni_2P Bifunctional Electrode. *Angewandte Chemie International Edition* **2019,** *58*(35), 12014-12017.

S37 Ding, Y.; Miao, B.-Q.; Li, S.-N.; Jiang, Y.-C.; Liu, Y.-Y.; Yao, H.-C.; Chen, Y., Benzylamine oxidation boosted electrochemical water-splitting: Hydrogen and benzonitrile co-production at ultra-thin Ni_2P nanomeshes grown on nickel foam. *Applied Catalysis B: Environmental* **2020,** *268*, 118393.